TECHNICAL REPORT ARCCB-TR-98019

SHOT-BY-SHOT EROSION MODELING OF RETIRED 120-MM M256 GUN TUBE #1988

S. SOPOK
P. VOTTIS
P. O'HARA
G. PFLEGL
C. RICKARD

OCTOBER 1998

DISCLAIMER

The findings in this report are not to be construed as an official Department of the Army position unless so designated by other authorized documents.

The use of trade name(s) and/or manufacturer(s) does not constitute an official indorsement or approval.

DESTRUCTION NOTICE

For classified documents, follow the procedures in DoD 5200.22-M, Industrial Security Manual, Section II-19 or DoD 5200.1-R, Information Security Program Regulation, Chapter IX.

For unclassified, limited documents, destroy by any method that will prevent disclosure of contents or reconstruction of the document.

For unclassified, unlimited documents, destroy when the report is no longer needed. Do not return it to the originator.

REPORT DOCUMENTATION PAGE

Form Approved
OMB No. 0704-0188

1. AGENCY USE ONLY (Leave blank)	2. REPORT DATE	3. REPORT TYPE AND DATES COVERED
	October 1998	Final

4. TITLE AND SUBTITLE

SHOT-BY-SHOT EROSION MODELING OF
RETIRED 120-MM M256 GUN TUBE #1988

5. FUNDING NUMBERS

AMCMS No. 6226.24.H180.0
PRON No. 4A8A8FYK1ABJ

6. AUTHOR(S)
S. Sopok, P. Vottis, P. O'Hara, G. Pflegl, and C. Rickard

7. PERFORMING ORGANIZATION NAME(S) AND ADDRESS(ES)

U.S. Army ARDEC
Benet Laboratories, AMSTA-AR-CCB-O
Watervliet, NY 12189-4050

8. PERFORMING ORGANIZATION REPORT NUMBER

ARCCB-TR-98019

9. SPONSORING/MONITORING AGENCY NAME(S) AND ADDRESS(ES)

U.S. Army ARDEC
Close Combat Armaments Center
Picatinny Arsenal, NJ 07806-5000

10. SPONSORING/MONITORING AGENCY REPORT NUMBER

11. SUPPLEMENTARY NOTES
Presented at the 34th AIAA Joint Propulsion Conference, Cleveland, OH, 13-15 July 1998.
Published in proceedings of the conference.

12a. DISTRIBUTION/AVAILABILITY STATEMENT
Approved for public release; distribution unlimited.

12b. DISTRIBUTION CODE

13. ABSTRACT (Maximum 200 words)

As our gun erosion database increases for in-service and out-of-service 120-mm M256 tubes with M829Ax series rounds, distinct erosion patterns and mechanisms are emerging. Variability exists for M256 guns with M829Ax series rounds depending on round count, round type, round-conditioning temperature, and their order. Our M256/M829Ax gun system erosion model—with its interior ballistics, thermochemistry, and boundary layer components—is constantly being guided and refined by the erosion and materials analysis data from fired gun tubes. A recent refinement includes the improvement of the gun steel subsurface exposure model due to high quality, difficult to obtain data from in-service M256 tubes. Other recent refinements to the boundary layer heat transfer model are based on thermal data from M256 tubes. These refinements include the improvement/incorporation of case gas cooling effects, turbulent gas mixing/heating effects, and a very minor contribution from forcing cone-induced vena contracta cooling effects. These latter refinements are calibrated away from crack walls by positional thermal wall repacking depth, thermal wall transformation depth, and thermocouple data. A comprehensive gun erosion model is described for the 120-mm M256 gun with its M829Ax series rounds. In addition, a detailed shot-by-shot erosion modeling prediction is described for retired 120-mm M256 gun tube serial #1988. For this gun tube, the erosion prediction includes the two types of rounds fired, M829 and M829A2, and their three round-conditioning temperatures, hot, ambient, and cold. The gun erosion mechanism consists of heat checking the inert chromium plate, subsequent interfacial degradation of the subsurface gun steel substrate at the chromium crack bases, then chromium platelet spalling, and subsequent bare gun steel gas wash. This gun erosion model correctly calculates and predicts that the worst eroded region is at 1.2 to 2.4 meters from the rear face of the tube. The excessive muzzle wear is by a different, purely mechanical gas wash-free mechanism. Most importantly, given herein are the relative erosion-related effective full-charge values of the fielded M256 gun kinetic energy rounds at various round-conditioning temperatures.

14. SUBJECT TERMS
Shot-by-Shot Gun Erosion Modeling, 120-mm M256 Cannon,
M829A2 Rounds, M829 Rounds

15. NUMBER OF PAGES
20

16. PRICE CODE

17. SECURITY CLASSIFICATION OF REPORT	18. SECURITY CLASSIFICATION OF THIS PAGE	19. SECURITY CLASSIFICATION OF ABSTRACT	20. LIMITATION OF ABSTRACT
UNCLASSIFIED	UNCLASSIFIED	UNCLASSIFIED	UL

TABLE OF CONTENTS

LIST OF ILLUSTRATIONS

INTRODUCTION

The existence of thermal-chemical-mechanical gun barrel erosion is documented in U.S. Army reports (ref 1). Numerous ADPA Tri-Service sponsored gun erosion meetings have implied a thermal-chemical-mechanical gun barrel erosion mechanism (ref 2). A unified computer model for predicting thermal-chemical-mechanical erosion in gun barrels was first described by Dunn et al. in 1995 (ref 3) using the following codes:

- Standard heat transfer modified by mass addition to boundary layer rocket code modified for guns (MABL)

- Standard nonideal gas-wall thermochemical rocket code modified for guns (CCET)

- Standard wall material ablation conduction erosion rocket code modified for guns (MACE)

Additionally, this gun barrel erosion model requires the standard interior ballistics gun code (XNOVAKTC) (ref 4) for input. To the degree available, our practical approach to gun barrel erosion modeling is kept on-track with actual experimental gun system data. As our gun erosion database increases, our gun erosion model evolves to include identifiable patterns.

The purpose of this report is to describe our comprehensive gun erosion model for the 120-mm M256 gun with its M829Ax series rounds. In addition, a detailed shot-by-shot erosion modeling prediction is described for retired 120-mm M256 gun tube serial #1988.

PROCEDURE

A comprehensive gun erosion model was developed for the 120-mm M256 gun with its M829Ax series rounds. Many types of experimental data were used to keep this gun erosion model on-track including:

- Pressure gauge
- Radar
- Thermal repacking (recrystallization) depth away from cracks (chromium plate, ~1300°K)
- Thermal transformation depth away from cracks (gun steel, ~1000°K)
- Thermocouple
- Kinetic rate function
- Subsurface metallographic and borescope data

Initial 120-mm M256 gun tube serial #1988 erosion modeling included the XNOVAKTC interior ballistic analysis for gas pressure, gas temperature, and gas velocity core flow data (ref 4). This initial step was followed by the MABL boundary layer recovery enthalpy/cold wall heat flux analysis and the CCET thermochemistry inert wall enthalpy/reacting wall enthalpy/ablation potential analysis (ref 3). The final step included the MACE wall temperature/erosion profile analysis (ref 3). Specifically, a detailed shot-by-shot erosion modeling prediction is described for this retired gun tube. This erosion prediction includes the two types of rounds fired—M829 and M829A2—and their three round-conditioning temperatures—hot = 49°C, ambient = 21°C, and cold = -32°C.

RESULTS AND DISCUSSION

For the subject gun tube, Figure 1 summarizes the XNOVAKTC interior ballistic analysis for maximum values of gas pressure (P_g), gas temperature (T_g), and gas velocity (V_g) for its M829 and M829A2 rounds as a function of axial position and round-conditioning temperature. Maximum values were used instead of time-dependent data to simplify the appearance of this figure. Selected axial positions included 0.69, 1.55, 2.18, 3.30, and 5.11 meters from the rear face of the tube (RFT), while the selected round-conditioning included hot (49°C), ambient (21°C), and cold (-31°C) temperatures. (These five selected axial positions and three selected round-conditioning temperatures will be used exclusively for the rest of the figures in this report.) Experimental pressure-time and muzzle velocity data were used to calibrate the interior ballistic analysis. In Figure 1, the T_g and P_g values decrease with increasing axial position, while the V_g values increase with increasing axial position for the bore region.

Figure 2 summarizes the M829 and M829A2 MABL analysis for maximum values of recovery enthalpy (H_r) and cold wall heat flux (Q_{cw}) as a function of the selected axial positions and round-conditioning temperatures. Maximum values were also used instead of time-dependent data to simplify the appearance of this figure. Experimental thermal repacking depth away from cracks, thermal transformation depth away from cracks, and thermocouple data were used to calibrate this improved boundary layer analysis. The figure illustrates that H_r and Q_{cw} values increase with increasing axial position for the 0.6 to 1.2 meter from RFT region; both values peak in the 1.2 to 2.4 meter range; then both values decrease with increasing axial position to the muzzle. Note that the heat transfer pattern in Figure 2 significantly differs from the core flow pattern in Figure 1 and cannot be solely explained on the basis of simple heat transmission (film) coefficient effects (ref 5). We theorize that this difference can be explained by an improved boundary layer analysis, including significant combustion case gas cooling effects and these significant turbulent gas mixing/heating effects.

Without combustion case gas cooling effects and turbulent gas mixing/heating effects, the 0.6 to 1.2-meter region would be the highest wall heat transfer region, but with both of these effects, the 1.2 to 2.4 meter region is the highest wall heat transfer region. The combustion case gas cooling effect is similar to transpiration, slot injection, and pure fuel injection cooling at the wall for rocket chambers, as well as ablative cooling at the wall for guns.

Combustible case gases were approximately 1600°K maximum for the M829 and M829A2 rounds, while their respective propellant core flow gases were approximately 3000°K and 3300°K maximum for these rounds. The combustible case ablates and its cooler gases (compared to the core flow) stay along the wall providing a cooled boundary layer from the onset of the bore at 0.6 meter from RFT to where it changes over to highly turbulent in the 1.2 to 2.4 meter from RFT region. This cooling reduces heat transfer to the wall and diminishes with increasing axial position. For the bore region, the increasingly turbulent boundary layer is due to geometry and flow field conditions that are characterized by a transition from turbulent microscopic fluid mixing to highly turbulent macroscopic fluid mixing.

For the M829 and M829A2 rounds, a combination of M256 gun chamber, forcing cone, and bore geometry induce a very minor vena contracta flow from the 0.6 meter from RFT onset of the bore to the 1.2 to 2.4 meter from RFT region. This type of flow exhibits slightly slower velocities in the boundary layer, thus slightly reducing heat transfer to the wall, then diminishing with increasing axial position.

Figure 3 summarizes the M829 and M829A2 CCET thermochemical analysis of reacting wall enthalpy (H_w) and ablation potential (B_a) (ref 3) for tube #1988 as a function of wall temperatures (T_{wall}) for high contraction (HC) chromium plate/A723 gun steel wall materials. Experimental kinetic rate function data and subsurface metallographic data were used to calibrate the thermochemical analysis and transform the chemical equilibrium analysis into a partial chemical kinetic analysis. The respective HC chromium maximum T_{wall}'s are about 1600°K and 1650°K for the M829 and M829A2 rounds. These are below its passivating oxidation temperature at about 2000°K and well below its melting point at about 2130°K, which explains its inertness. The respective A723/iron maximum T_{wall}'s are about 1375°K and 1400°K for the same M829 and M829A2 rounds. These are well above its rapid expansive flaking oxidation temperature at about 1055°K, explaining its reactivity. In addition, they are below its iron oxide melting point at about 1640°K and well below its A723/iron melting point at about 1810°K.

Figure 4 summarizes the M829 and M829A2 borescope data analysis of A723 subsurface exposure through HC chromium plate cracks as a function of rounds fired for selected axial positions. The experimental borescope data was used to calibrate the erosion analysis. This data was collected on a cleaned M256 tube that had about half M829A2 and half M829 rounds. These M829A2 and M829 rounds consisted of a nearly equal distribution of hot, ambient, and cold temperature conditioning. Data collection involved the use of a magnifying borescope with a calibrated scale to measure the number and average area of each HC chromium platelet within a designated total area as a function of axial position for a given round count.

We were able to collect high quality borescope data from approximately half M829 and half M829A2 rounds on a single M256 tube near its 50-round point, near its 150-round point, and at its final out-of-service round point. The balance of the M829 rounds was converted to effective M829A2 rounds. The initial zero-round condition data were not collected from this M256 tube, but from the many unfired M256 tubes available at Watervliet Arsenal. High contraction chromium plate has fine cracking and finite shrinkage when manufactured and prior

3

to firing. To date, it has been a difficult feat to collect in-service M256/M829Ax series borescope data and then continue to follow that tube until it is taken out of service. Regarding tube #1988 borescope data, we recognize that this is a sample of one and that significant variability exists depending on combinations of round count, round type, round-conditioning temperature, and their firing order.
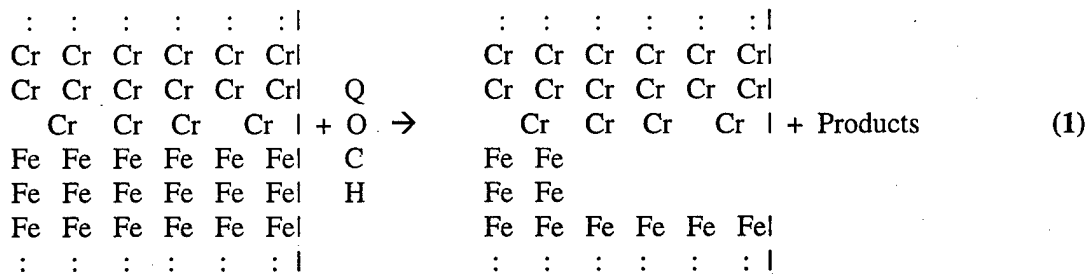
For the selected axial positions in Figure 4, from 50 to 125 rounds, the A723 subsurface exposure rose rapidly due to HC chromium thermal repacking, nonmetallic out-gassing, and possibly compression resulting in its shrinkage and heat checking. After about 125 rounds, the above mechanism diminished and A723 subsurface exposure rose more slowly because only the HC chromium platelet spalling mechanism remained. At the 5.11 meter from RFT near-muzzle position, the A723 subsurface exposure rose very rapidly from about 125 rounds until its out-of-service round count due to HC chromium platelet spalling by a different purely mechanical mechanism. This tube was taken out-of-service due to dispersion at about seventy percent of its estimated erosion life possibly because of the typical severe muzzle wear.

Figure 5 presents two typical 100x metallographs of M256 tube #1988 with about half M829A2 and half M829 rounds at 0.69 meter from RFT. This represents the 0.6 to 1.2 meter region, and was used to calibrate the erosion analysis. The 0.6 to 1.2 meter region has the highest gas pressure of any bore region (Figure 1), which explains the deep crack depths due to severe dilation. Although this 0.6 to 1.2 meter region has the highest gas temperature of any bore region (Figure 1), heat transfer to the wall is significantly diminished due to combustion case gas cooling effects (Figure 2). These observations explain the heat checking and crack spacing as well as the near absence of interface degradation and chromium platelet spalling.

Figure 6 presents two typical 100x metallographs of M256 tube #1988 with about half M829A2 and half M829 rounds at 1.55 meters from RFT. This represents the 1.2 to 2.4 meter region and was also used to calibrate the erosion analysis. The 1.2 to 2.4 meter region has a lower gas pressure than the 0.6 to 1.2 meter region (Figure 1), which explains the moderate crack depths due to moderate dilation. Although this 1.2 to 2.4 meter region has a lower gas temperature than the 0.6 to 1.2 meter bore region (Figure 1), heat transfer to the wall is significantly higher due to turbulent gas mixing (Figure 2). These observations explain the heat checking and crack spacing as well as the prevalent interface degradation and chromium platelet spalling. We theorize that the main gun erosion mechanism consists of inert chromium plate cracking, shrinkage, and heat checking, followed by subsequent interfacial degradation of the subsurface gun steel substrate at the chromium crack bases, subsequent chromium platelet spalling, and subsequent bare gun steel gas wash. The gun steel at the chromium/gun steel interface is more susceptible to interface degradation than either of its components separately due to its higher energy state and reactivity. In addition, interface degradation is enhanced by expansive flaking of iron oxide.

As chromium platelets detach from the substrate and rise above attached chromium platelets, they are more susceptible to mechanical removal by the projectile. In addition, the 1.2 to 2.4 meter region has a wavy chromium surface appearance in cross-section due to partially detached chromium platelets. Rarely do radial heat-checking cracks link-up to spall a chromium platelet with attached gun steel. Although there appears to be evidence of heat-checking cracks extending into the wall well beyond the heat-affected zone due to environmental-assisted cracking, great scrutiny has produced no measurable evidence of chromium platelet spalling due to cracking in the plane of the chromium plate/gun steel interface.

Below is a detailed summary of our hot gas erosion theory and its relationship to the above calculations and empirical data. Equation 1 depicts the A723 gun steel/HC chromium plate interface as-plated (left) and with in-progress interface degradation (right). Nonequilibrium HC chromium plate shrinks and cracks widen by thermal repacking and out-gassing. The vertical dashed line is one side of a radial crack wall. The first chromium plated interface layer and the iron degradation layer are actually multiple atomic layers. Gun steel interface degradation is dominated by the recurring formation and removal of a thin surface layer of measurable untempered martensite, a thin surface layer of measurable oxidation, a somewhat thicker layer of measurable interstitially diffused carbon, and theoretically a thicker layer of unmeasurable interstitially diffused hydrogen. Oxidation of gun steel wall iron can occur in a moderately reducing combustion gas environment, since oxygen has more of an affinity for iron metal than it does for partially oxidized gas species. The chromium/gun steel interface and the resultant gun steel interface surface produced by interface degradation are in excess of ninety-five percent iron, and are at higher energy and more susceptible to damage from oxygen, carbon, and hydrogen than the bulk iron. High concentrations of damaging oxygen and carbon products have been measured at the iron interface. In addition, carbon and hydrogen products diffuse into and embrittle the gun steel.

$$
\begin{array}{llllll}
: & : & : & : & : & :| \\
Cr & Cr & Cr & Cr & Cr & Cr| \\
Cr & Cr & Cr & Cr & Cr & Cr| & \quad Q \\
& Cr & Cr & Cr & & Cr~| & +~O \\
Fe & Fe & Fe & Fe & Fe & Fe| & \quad C \\
Fe & Fe & Fe & Fe & Fe & Fe| & \quad H \\
Fe & Fe & Fe & Fe & Fe & Fe| \\
: & : & : & : & : & :|
\end{array}
\rightarrow
\begin{array}{llllll}
: & : & : & : & : & :| \\
Cr & Cr & Cr & Cr & Cr & Cr| \\
Cr & Cr & Cr & Cr & Cr & Cr| \\
& Cr & Cr & Cr & & Cr~| & +~Products \\
Fe & Fe & & & & \\
Fe & Fe & & & & \\
Fe & Fe & Fe & Fe & Fe & Fe| \\
: & : & : & : & : & :|
\end{array}
\qquad (1)
$$

Metal-metal bonds have an equilibrium energy balance between attractive and repulsive forces that determines the activation energy necessary to break these bonds. If the local system energy increases, then this activation energy is easier to achieve.

Our gun erosion code wall heat transfer and wall temperature model has provided the following information:

- Bore surface temperatures for chromium plate and exposed gun steel (after chromium platelet spalling) from turbulent convection

- Radial crack wall surface and interface temperatures for chromium plate and gun steel from turbulent convection and conduction

- Bore surface and chromium/gun steel interface temperatures away from a radial crack for chromium plate and gun steel from conduction alone

At the 0.6 to 1.2 meter region, the chromium/gun steel interface, resultant gun steel interface surface due to interface degradation, and resultant gun steel surface due to chromium spalling typically exhibit deep radial crack depth and little erosion. The minimal erosion is mainly attributed to gun steel interface degradation, although less than five percent is attributed to radial crack linkage erosion. At this region, gas pressure is high, gas temperature is high, gas velocity is low, the boundary layer is thick, subsurface exposure is moderate, hot gas convective heat transfer is mildly turbulent at the surface, hot gas convective heat transfer is borderline turbulent in the axial direction radial cracks, and hot gas convective heat transfer is nonturbulent in the circumferential direction radial cracks. These conditions allow conductive heating to dominate the gun steel interface temperature values at the radial crack walls. For this region, the respective relationships between the gas, surface, and crack wall interface temperatures are ~1.0x and ~0.3x.

At the 1.2 to 2.4 meter region, the chromium/gun steel interface, resultant gun steel interface surface due to interface degradation, and resultant gun steel surface due to chromium spalling typically exhibit moderate radial crack depth and significant erosion. This erosion is mainly attributed to gun steel interface degradation, although less than five percent is attributed to radial crack linkage erosion. At this region, gas pressure is moderate, gas temperature is moderate, gas velocity is high, the boundary layer is thin, subsurface exposure is high, hot gas convective heat transfer is highly turbulent at the surface, hot gas convective heat transfer is moderately turbulent in the axial direction radial cracks, and hot gas convective heat transfer is nonturbulent in the circumferential direction radial cracks. These conditions allow convective heating to dominate the gun steel interface temperature values at the radial crack walls. For this region, the respective relationships between the gas, surface, and crack wall interface temperatures are ~1.0x and ~0.5x. Conduction alone into the wall away from the radial crack wall surface is a bad indicator of erosion, since it ignores the important turbulent convective element at the radial crack wall surface.

Figure 7 summarizes the M256 tube #1988's distribution of M829 and M829A2 round types and hot/ambient/cold round-conditioning temperatures, which are the same as those in Figure 1.

Figure 8 shows the subject tube's MACE wall temperature profile analysis for HC chromium maximum surface temperature (T_{wall}) as a function of round-conditioning temperatures for selected axial positions and round types. The respective HC chromium maximum T_{wall}'s are about 1600°K and 1650°K for the M829 and M829A2 rounds. These are below its passivating oxidation temperature at about 2000°K and well below its melting point at about 2130°K, thus explaining its inertness.

Figure 9 shows the tube's MACE wall temperature profile analysis for A723 maximum interface and surface wall temperatures (T_{wall}) as a function of round-conditioning temperatures for selected axial positions and round types. The A723 maximum interface T_{wall} values are a combination of convection and conduction at the crack walls. The respective A723/iron maximum interface T_{wall}'s are about 1225°K and 1250°K for the M829 and M829A2 rounds. These are above its rapid expansive flaking oxidation temperature at about 1055°K, explaining its reactivity. In addition, they are below its iron oxide melting point at about 1640°K and well below its A723/iron melting point at about 1810°K. Diffusion, reactions, transformations, and gas wash thermochemically degrade interfacial A723 at HC chromium plate heat-checked crack bases. The respective A723/iron maximum surface T_{wall}'s are about 1375°K and 1400°K for the M829 and M829A2 rounds. These are well above its rapid expansive flaking oxidation temperature at about 1055°K, explaining its reactivity. In addition, they are below its iron oxide melting point at about 1640°K and well below its A723/iron melting point at about 1810°K. Diffusion, reactions, transformations, and gas wash thermochemically degrade fully exposed surface A723 after HC chromium plate spalling.

Figures 8 and 9 show that wall temperature profiles follow the positional order of the heat transfer pattern from Figure 2. In these two figures, maximum values were used instead of time-dependent data to simplify their appearance. Also, experimental thermal repacking depth away from cracks, thermal transformation depth away from cracks, and thermocouple data were used to calibrate calculated wall temperature profiles.

Figure 10 summarizes the MACE cumulative erosion analysis for tube #1988 as a function of cumulative rounds for selected axial positions. Tube #1988 was taken out-of service for excessive dispersion at 424 rounds, which is about seventy percent of its estimated erosion life. This figure shows the 2.18 meter from RFT axial position to be the most eroded position. It takes about 170 rounds for chromium platelet spalling onset/gun steel gas wash onset to occur, and it takes 424 rounds to achieve about 3 mm of cumulative erosion. This is typical erosion damage for this gun system when taken out-of-service by dispersion. If this gun tube had remained in service, it should have lasted an estimated 550 to 600 rounds before being condemned by erosion at 5-mm depth.

In Figure 10 cumulative wall erosion profiles also follow the positional order of the heat transfer pattern from Figure 2. Erosion life is lowest at 2.18 meters, higher at 1.55 meters, still higher at 0.69 meter, higher yet at 3.30 meters, and highest at 5.11 meters from RFT. Additionally, the figure shows that interface life follows this same pattern with the exception of the 5.11 meter position, which is believed to be by a different mechanism.

The erosion mechanism consists of:

- Heat checking of the inert chromium plate
- Subsequent interfacial degradation of the subsurface gun steel substrate at the chromium crack bases
- Subsequent chromium platelet spalling
- Subsequent bare gun steel gas wash

Mechanisms of interface degradation include diffusion, reactions (i.e., expansive oxidation), transformations, and gas wash. This overall gun erosion analysis correctly predicts that the worst eroded region is located at 1.2 to 2.4 meters from RFT. The excessive gas wash-free muzzle wear is by a different purely mechanical mechanism. Our overall gun erosion analysis correctly predicts the following relative distribution of M256 erosion-related effective full-charge values: if M829 at -32°C = 1.0, then M829 at 21°C = 1.5, M829 at 49°C = 2.2, M829A1 at -32°C =1.3, M829A1 at 21°C = 1.9, M829A1 at 49°C = 2.8, M829A2 at -32°C =1.5, M829A2 at 21°C = 2.3, and M829A2 at 49°C = 3.4. Traditionally, all M256 effective full-charge values have been equal to one per the U.S. Army Evaluation of Cannon Tubes Technical Manual.

REFERENCES

1. Alkidas, A., Morris, S., Christoe, C., Caveny, L., and Summerfield, M., "Erosive Effects of Various Pure and Combustion-Generated Gases on Metals - Part II," U.S. Army Materials and Mechanics Research Center, Watertown, MA, 1977; see also Part I, 1975.

2. Picard, J., Ahmad, I., and Bracuti, A., *Proceedings of the Tri-Service Gun Tube Wear and Erosion Symposiums*, U.S. Army ARDEC/ADPA, Dover, NJ, 1970, 1972, 1977, and 1982.

3. Dunn, S., Sopok, S., Coats, D., O'Hara, P., Nickerson, G., and Pflegl, G., "Unified Computer Model for Predicting Thermochemical Erosion in Gun Barrels," *Proceedings of 31st AIAA Propulsion Conference*, San Diego, CA, July, 1995.

4. Gough, P., "The XNOVAKTC Code," Paul Gough Associates, Portsmouth, NH, 1990.

5. Corner, J., *Theory of the Interior Ballistics of Guns*, John Wiley and Sons, New York, 1950.
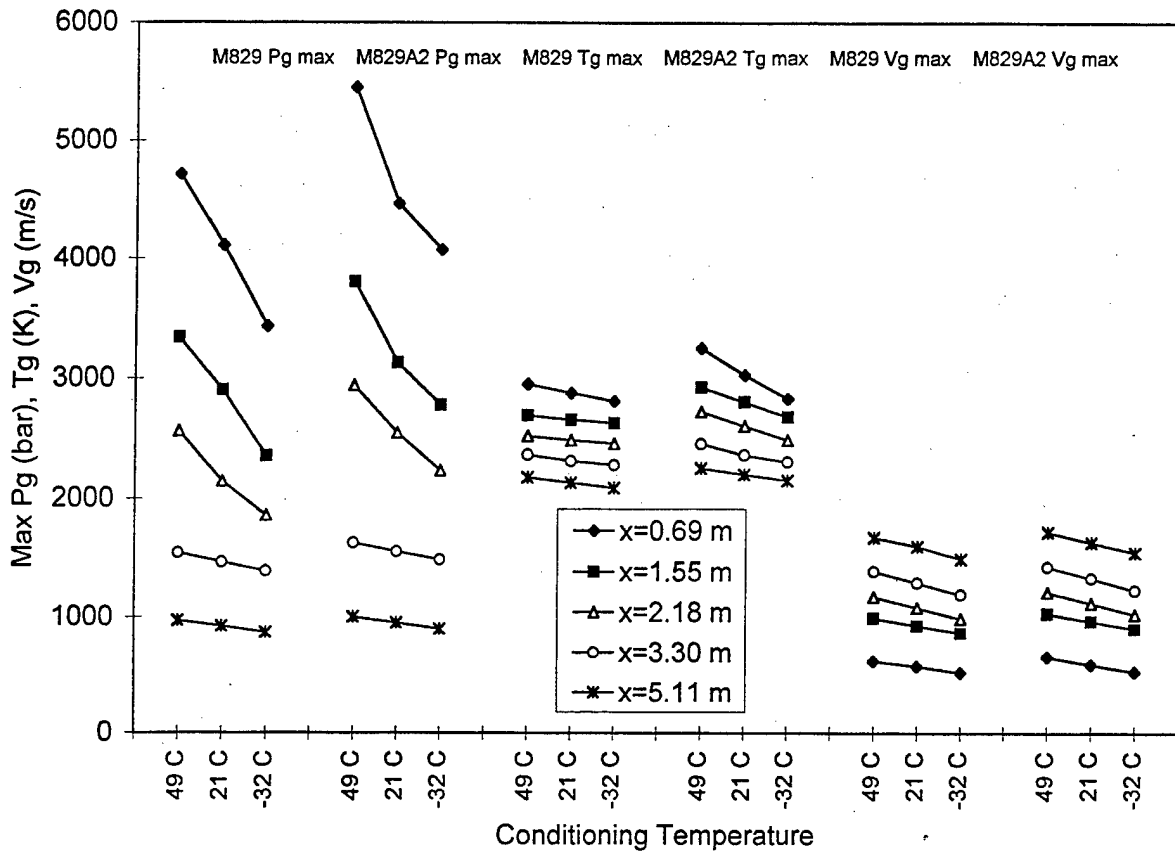
Figure 1. M829 and M829A2 calibrated interior ballistic analysis for maximum values of gas pressure, gas temperature, and gas velocity.
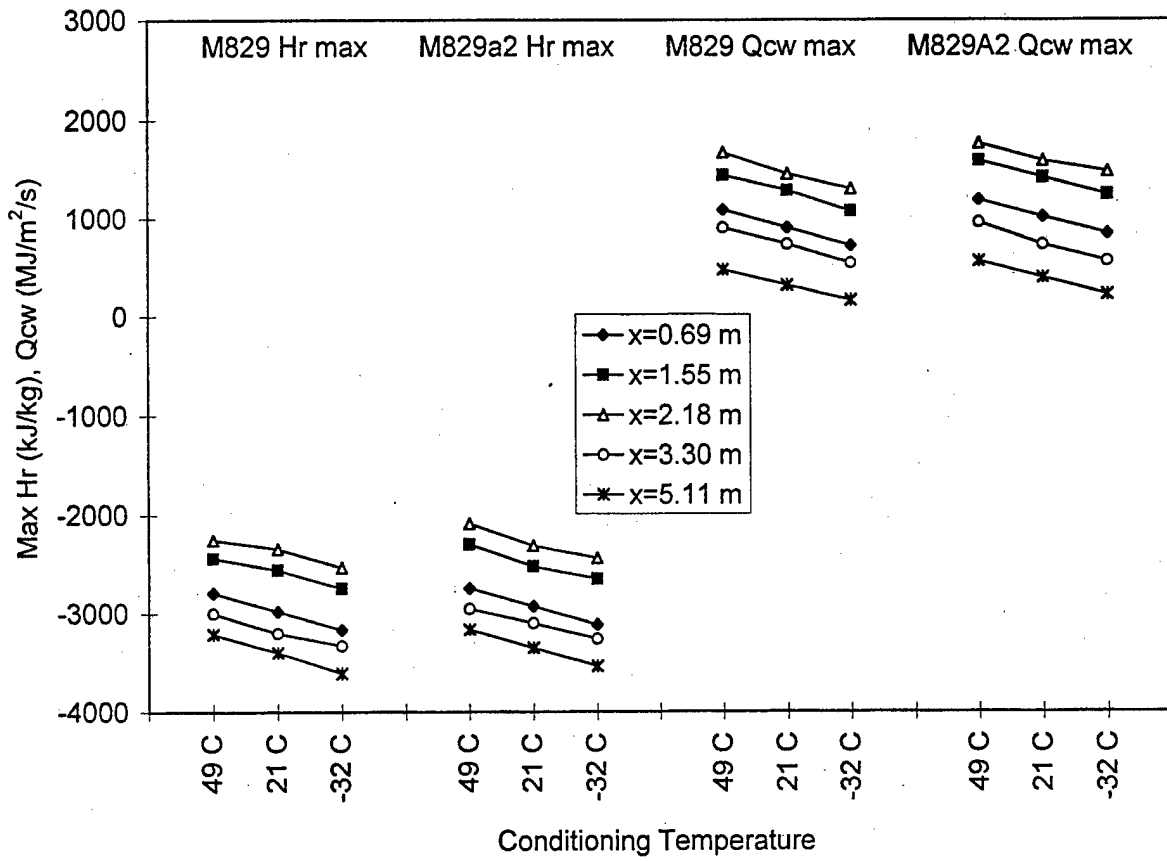
Figure 2. M829 and M829A2 calibrated MABL analysis for maximum values of recovery enthalpy and cold wall heat flux.
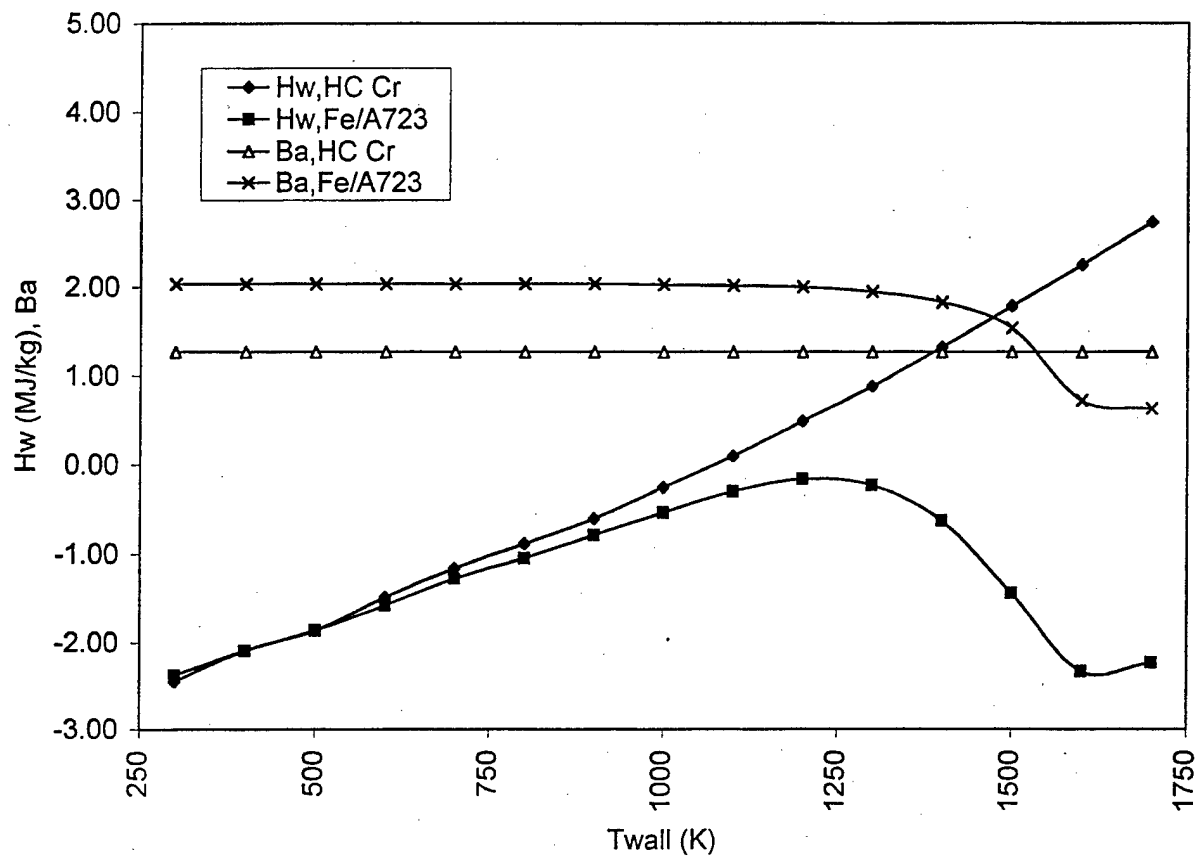
Figure 3. M829 and M829A2 calibrated CCET thermochemical
analysis of reacting wall enthalpy and ablation potential.
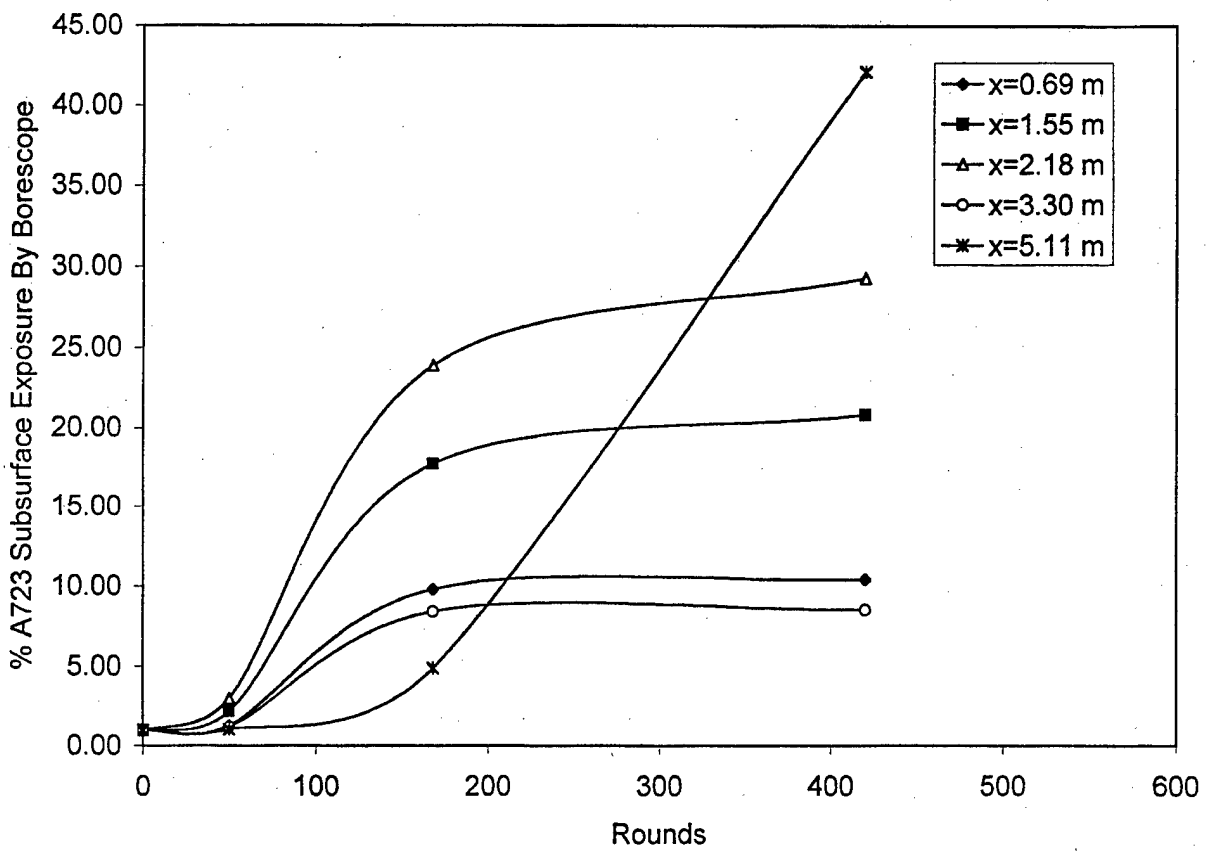
Figure 4. M256 tube #1988 borescope data analysis of
A723 subsurface exposure through HC chromium plate cracks.
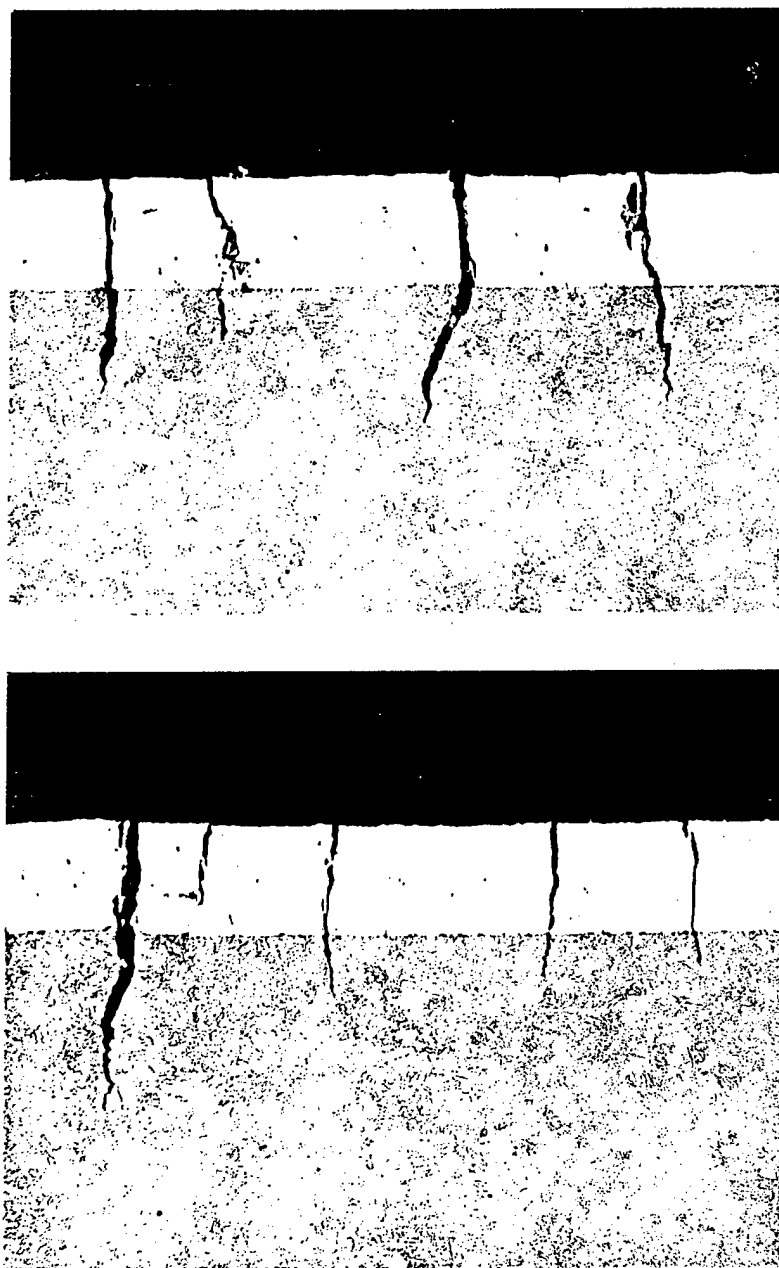
Figure 5. Tube #1988 metallographs at 0.69 meter
representing 0.6 to 1.2 meter region (100x).

14
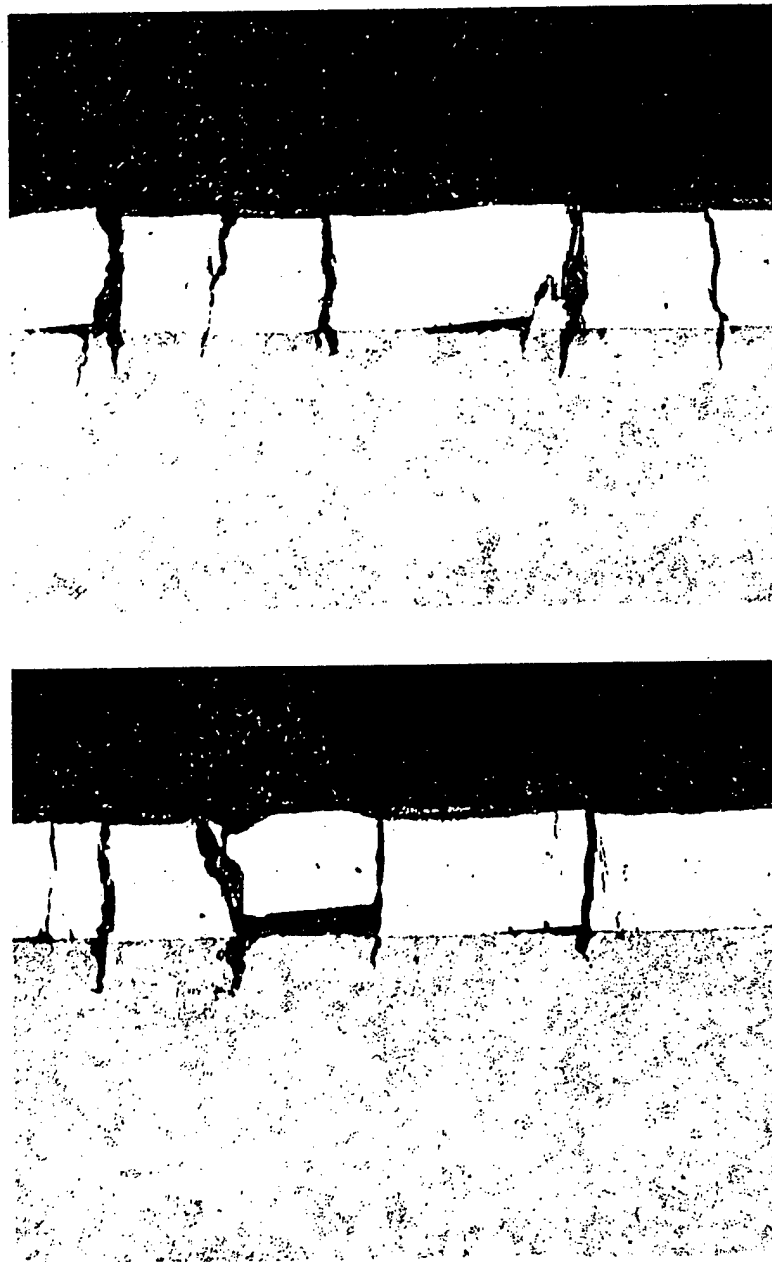
Figure 6. Tube #1988 metallographs at 1.5 meters
representing 1.2 to 2.4 meter region (100x).

15
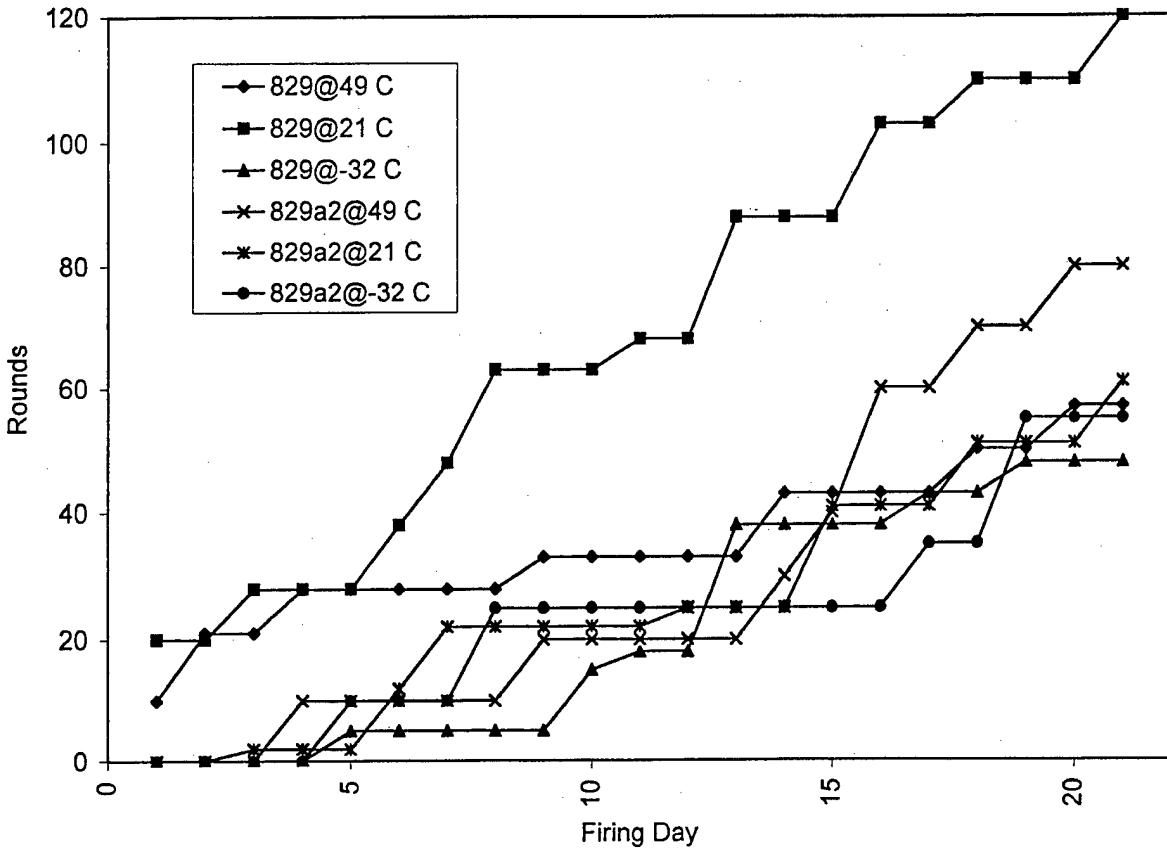
Figure 7. Tube #1988's distribution of M829 and M829A2 rounds
(424 total) and their hot/ambient/cold round-conditioning temperatures.
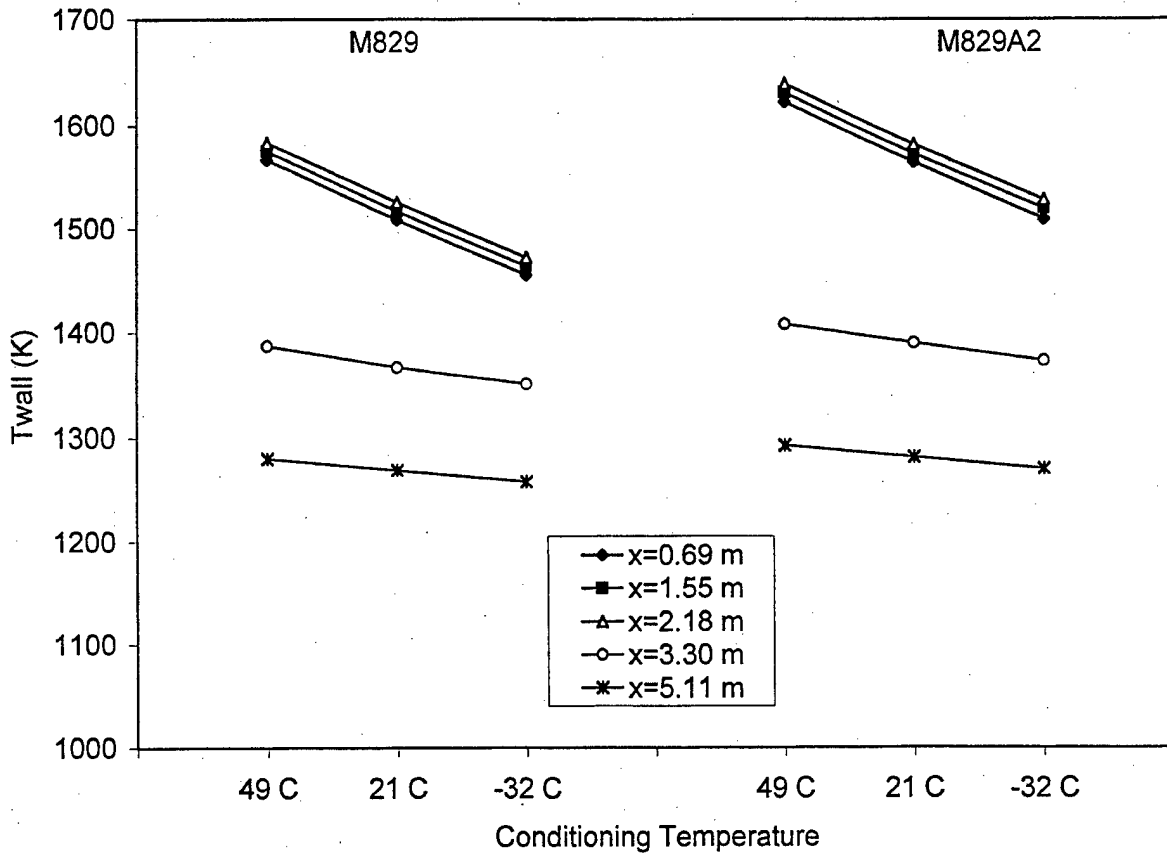
Figure 8. M256 tube #1988 calibrated MACE wall temperature profile analysis for HC chromium maximum surface temperature.
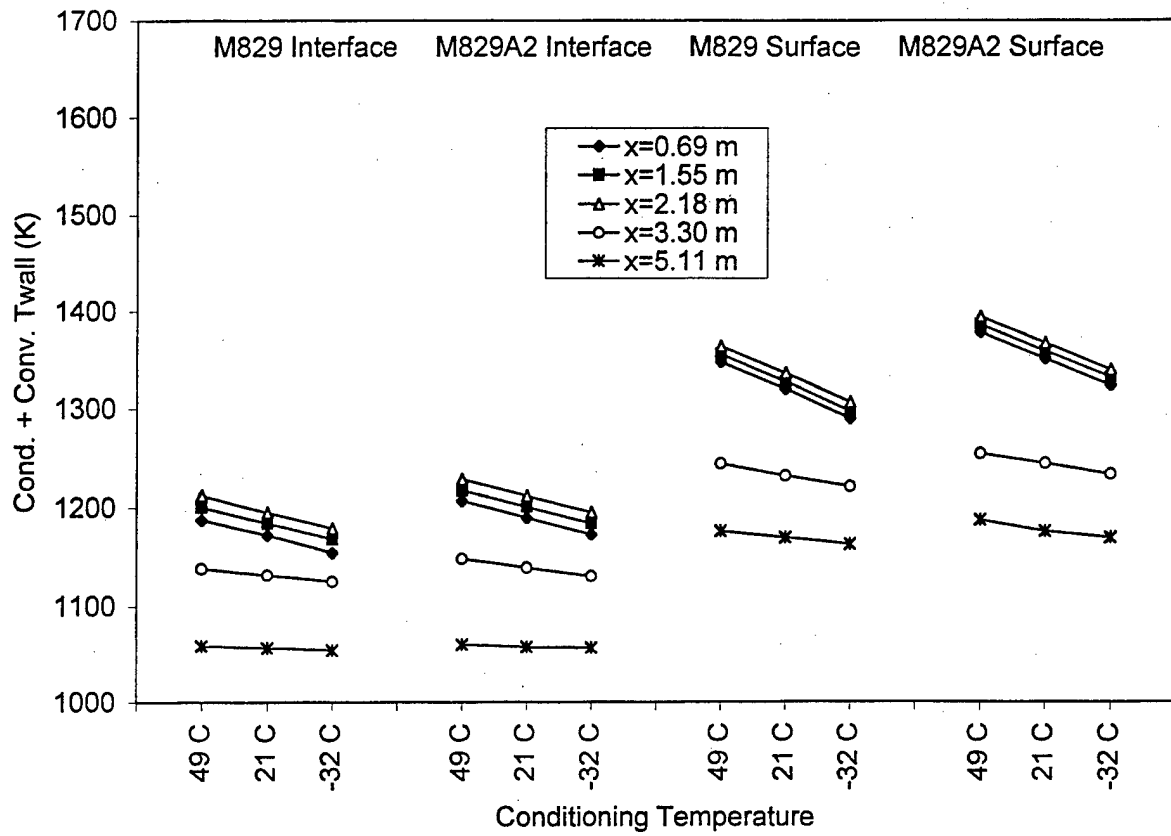
Figure 9. M256 tube #1988 calibrated MACE wall temperature profile analysis for A723 maximum interface and surface wall temperatures.
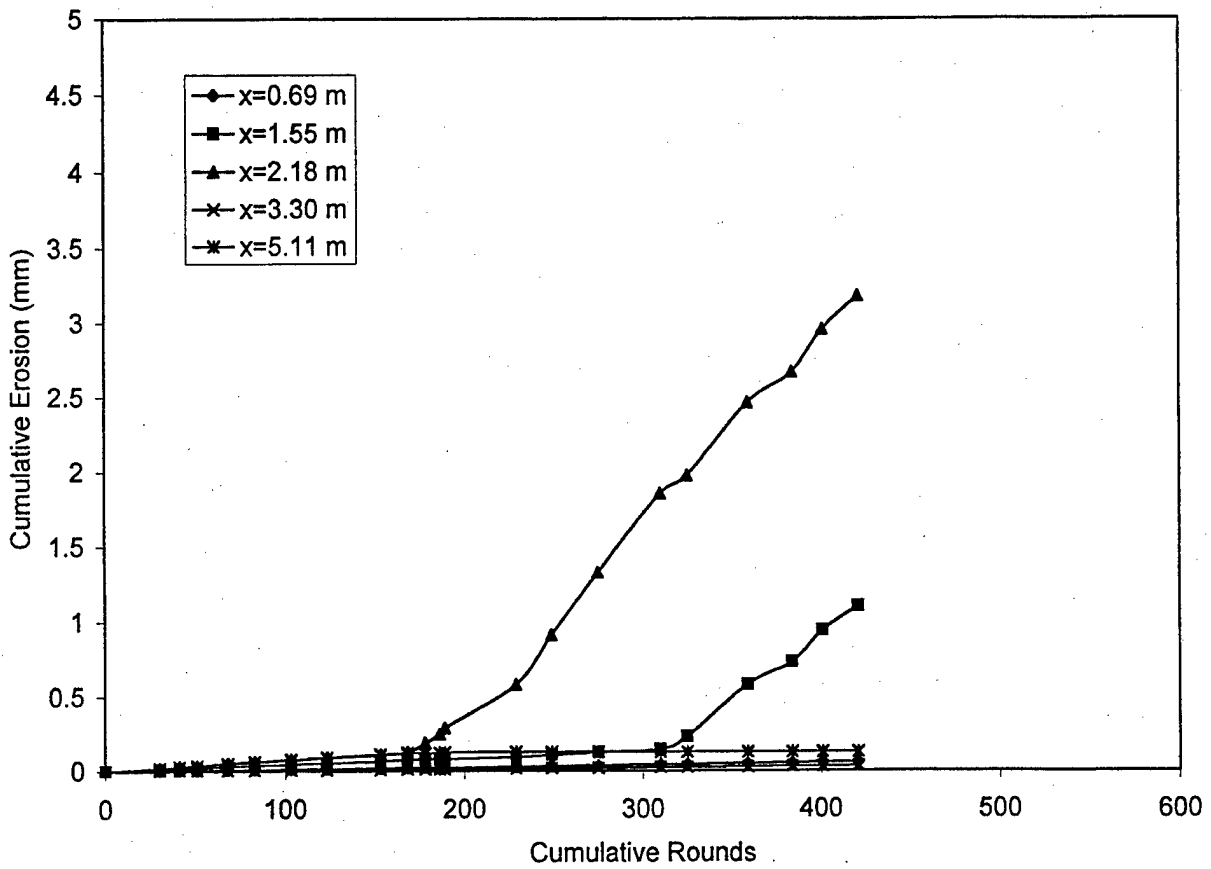
Figure 10. Summary of MACE cumulative erosion analysis for M256 tube #1988 as a function of cumulative rounds for selected axial positions.

TECHNICAL REPORT INTERNAL DISTRIBUTION LIST

	NO. OF COPIES
CHIEF, DEVELOPMENT ENGINEERING DIVISION	
ATTN: AMSTA-AR-CCB-DA	1
-DB	1
-DC	1
-DD	1
-DE	1
CHIEF, ENGINEERING DIVISION	
ATTN: AMSTA-AR-CCB-E	1
-EA	1
-EB	1
-EC	1
CHIEF, TECHNOLOGY DIVISION	
ATTN: AMSTA-AR-CCB-T	2
-TA	1
-TB	1
-TC	1
TECHNICAL LIBRARY	
ATTN: AMSTA-AR-CCB-O	5
TECHNICAL PUBLICATIONS & EDITING SECTION	
ATTN: AMSTA-AR-CCB-O	3
OPERATIONS DIRECTORATE	
ATTN: SIOWV-ODP-P	1
DIRECTOR, PROCUREMENT & CONTRACTING DIRECTORATE	
ATTN: SIOWV-PP	1
DIRECTOR, PRODUCT ASSURANCE & TEST DIRECTORATE	
ATTN: SIOWV-QA	1

NOTE: PLEASE NOTIFY DIRECTOR, BENÉT LABORATORIES, ATTN: AMSTA-AR-CCB-O OF ADDRESS CHANGES.

TECHNICAL REPORT EXTERNAL DISTRIBUTION LIST

NOTE: PLEASE NOTIFY COMMANDER, ARMAMENT RESEARCH, DEVELOPMENT, AND ENGINEERING CENTER, BENÉT LABORATORIES, CCAC, U.S. ARMY TANK-AUTOMOTIVE AND ARMAMENTS COMMAND, AMSTA-AR-CCB-O, WATERVLIET, NY 12189-4050 OF ADDRESS CHANGES.

	NO. OF COPIES		NO. OF COPIES
COMMANDER U.S. ARMY RESEARCH OFFICE ATTN: CHIEF, IPO P.O. BOX 12211 RESEARCH TRIANGLE PARK, NC 27709-2211	1	WRIGHT LABORATORY ARMAMENT DIRECTORATE ATTN: WL/MNM EGLIN AFB, FL 32542-6810	1
DIRECTOR U.S. NAVAL RESEARCH LABORATORY ATTN: MATERIALS SCI & TECH DIV WASHINGTON, D.C. 20375	1	WRIGHT LABORATORY ARMAMENT DIRECTORATE ATTN: WL/MNMF EGLIN AFB, FL 32542-6810	1

NOTE: PLEASE NOTIFY COMMANDER, ARMAMENT RESEARCH, DEVELOPMENT, AND ENGINEERING CENTER, BENÉT LABORATORIES, CCAC, U.S. ARMY TANK-AUTOMOTIVE AND ARMAMENTS COMMAND, AMSTA-AR-CCB-O, WATERVLIET, NY 12189-4050 OF ADDRESS CHANGES.